A Reduced Order Thermal Model for Lithium Ion Batteries Derived from the Cahn-Hilliard Equation

R. Painter [1], I. Embry [1,] L. Sharpe [2], S. K. Hargrove [2],
[1] Department of Civil Engineering, Tennessee State University, Nashville, TN, USA
[2] Department of Mechanical Engineering, Tennessee State University, Nashville, TN, USA

Introduction

Fossil fuels play a significant role in the world economy since automobiles, trains, airplanes, and most power plants use fossil fuels. The continued demand for fossil fuels leads to severe problems like environmental pollution, climate change, and economic dependence on other nations. Renewable energy sources alleviate this problem to a certain extent, but they are not capable of generating large quantities of electricity relative to fossil fuels, and their supply can be unpredictable and inconsistent. Therefore, there is a need to develop new technologies which are consistent, have a high energy density, and have minimal effects on the environment. Emerging battery technologies are addressing these problems of renewable and fossil fuel energy sources since they can store and release energy on demand. In recent years significant strides have been made in lithium battery technology. Lithium batteries are the primary sources of power in modern-day applications, such as portable consumer electronics, electric and hybrid electric vehicles (EV and HEV), implantable electronic medical devices and space vehicles [1-4]. M. Stanley Whittingham, inventor of the lithium-ion battery for Exxon recently predicted that “within ten years, every vehicle will be hybrid or electric.” Because of technological advances, there is a lithium rush in battery technology reminiscent of the fossil fuel rush in the last century. In just a few years, thanks to battery advances, “the fossil-fueled car will be an aesthetic choice, not an economic necessity. And our city electric grids will be a lot more complicated yet more predictable, reliable and economical” [5].

Li-ion batteries do however have a significant drawback because its cycle life is shortened when operating at high or low temperatures. The battery capacity decreases significantly during operations at high temperatures due to irreversible chemical reactions [6]. If cell temperature is not monitored and controlled, a battery can experience a thermal runaway, with the risk of explosion [7, 8]. Vehicle applications require battery monitoring system (BMS) to not only protect Li-ion batteries from overheating and overcharging and over-discharging, but the BMS is also vital for formulating power management strategies that account for battery electrical and thermal performance limitations while minimizing fuel consumption and emissions. Thus, the lithium ion battery model incorporated in the BMS must provide accurate real-time knowledge of the battery’s temperature and its state-of-charge and voltage. A disadvantage common to dimensional physics-based Li-ion battery models are the long simulation time due to a large number of nonlinear equations, so these models become computationally inefficient for simulating conditions in real-time. Thus, a large body of research has ensued towards developing reduced-order models (ROM) for Li-ion batteries.

Equivalent-circuit models (ECM), which do not consider fundamental physics, have been widely used to mimic relationships between the battery input and output systems while providing real-time computation. [9-12]. ECM use electrical circuits to simulate Li-ion cells using capacitors to model the battery capacity while variable resistors and controlled voltage sources model the effect of temperature or SOC variations. Another widely applied approach for providing real time computation is black box modeling. Black body modeling relies on developing an equivalent transform function with multiple inputs and outputs. Like ECM this method relies on experimental data for a battery [13]. ECM and transform functions are usually implemented in a "mixed approach" combined with thermal and aging models in Figure 1 [14].

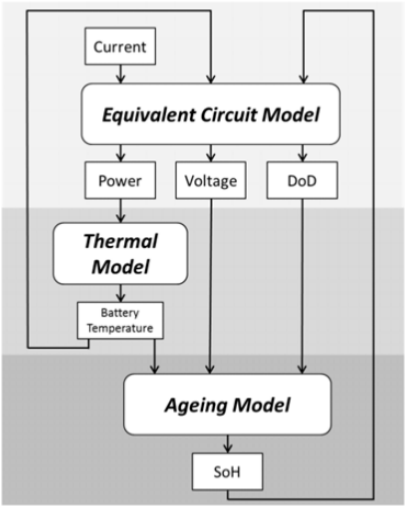

Figure 1 Equivalent Circuit Model Based Battery Management System

A significant drawback to these models has been that the states in the reduced-order system do not retain the physical meaning of the original system. The single particle (SP) model has been proposed to improve computational run time without compromising accuracy, [15,16]. In the single particle thermal model formulations, the local potential and concentration gradients in the electrolyte phase are ignored and accounted for using a lumped solution resistance terms [17-19]. Similarly, the potential gradients in the solid phase of the electrodes are also disregarded, and the porous electrode is treated as a large number of individual particles all being subjected to the same conditions. The single particle thermal

formulation accounts for ion transport in the electrode particles and the intercalation reaction kinetics.

Lithium iron phosphate ($LiFePO_4$) is the most commonly used phosphate-based cathode material for Li-ion batteries. $LiFePO_4$ has a strong tendency to separate into solid high Li+ concentration and low Li+ concentration phases, resulting in the batteries characteristic wide voltage plateau at room temperature. Initially, it was believed that LifePO4 was destined for only low rate applications due to its tendency for phase separation [20]. The now well-known high rate performance characteristics of the $LiFePO_4$ cathode came mostly from these advances: particle size reduction to nano-scale, carbon coating, incorporation of dopants, and diluting the cathode's active mass [21-25]. Traditionally mathematical models of intercalation dynamics in $LiFePO_4$ cathodes were based on a spherical diffusion or a shrinking core concept [26-28]. However, recent experimental and theoretical advances indicate a more realistic single particle (SP) model must account for phase equilibrium and nonequilibrium solid-solution transformations [29-33]. These advances are transforming the way we understand intercalation kinetics and ion transport in $LiFePO_4$.

In an actual battery, all particles do not simultaneously participate in the charging and discharging of the electrode. Beyond this, the study of $LiFePO_4$ at the mesoscale is an emerging field. Therefore, at the present, SP model parameters cannot be simply scaled up to bulk battery scales. The room temperature diffusivity of lithium in $LiFePO_4$ is reported in the literature as low as 10^{-16} and as high as 10^{-8} cm^2/s, and similarly, reported values of the exchange current density for $LiFePO_4$ also vary over several orders of magnitude. The most significant factor in these discrepancies is the misrepresentations associated with the relationships between the electrode's bulk, multiple particle, and single-particle scales [34]. The ROM presented below is a thermal model derived from a SP Cahn Hilliard simulation of the $LiFePO_4$ cathode. The ROM is developed and validated based on experimental electrical and thermal data and property data for an A123 Systems 26650, 2.3 Ah cylindrical battery [35].

Theory

We applied a 3D Cahn-Hilliard SP phase field model for LiFePO4 nanoparticles to serve as a test-bed for the development and verification of the ROM. The phase field model allowed estimation of the battery's voltage plateaus and also validated the voltage, SOC profiles as a function of temperature. A phase field model is necessary for modeling systems in which the diffuse interface is essential to the problem, such as spinodal phase decomposition. The model determines the chemical potential as a function of solid phase ion concentration. We assumed the particle was spherical and isotropic and did not consider particle surface wetting. The model equations are presented below where the overbar indicates dimensionless parameters and variables.
The diffusion chemical potential based on the regular solution model and derived from the Cahn-Hillard free energy functional is,

$$\bar{\mu} = -k_b T \mathrm{Ln}[\tfrac{\bar{c}}{1-c_m}] + \tfrac{\bar{\Omega}(c_m-\bar{c})}{c_m} - \tfrac{KV_s}{\mathrm{cm}}\bar{\nabla}^2\bar{c} \qquad \text{Eq. 1}$$

The basic evolution equation for mass conservation is,

$$\frac{\partial \bar{c}}{\partial \bar{t}} = -\bar{\nabla}.\bar{\mathrm{F}} \qquad \text{Eq. 2}$$

where $\bar{c}$ is the ion concentration and F is the ion flux. The ion flux is driven by the gradient of the diffusional chemical potential $\bar{\mu}$ as,

$$\bar{\mathrm{F}} = \tfrac{-D_O(c_m-\bar{c})}{k_m T c_m}\bar{\nabla}\bar{\mu}\,. \qquad \text{Eq. 3}$$

where D_O is the ion diffusivity and c_m is the maximum ion concentration, T is the absolute temperature, k_b is Boltzmann's constant, $\bar{\Omega}$ is the enthalpy of mixing per site, K is the gradient energy penalty coefficient and $V_s = 1/c_m$.
Voltage enters the Cahn- Hilliard SP model via Butler-Volmer kinetics derived from transition state theory for concentrated solutions [29] as

$$\bar{I} = \bar{I}_0[\exp(-\alpha\,\bar{\eta})\,i - \exp\big((1-\alpha)\bar{\eta}\big)]. \qquad \text{Eq. 4}$$

where α is the electron-transfer symmetry factor, and $\eta = \Delta\phi - \Delta\phi_{eq}$ is the surface overpotential due to the activation polarization, $\Delta\phi$ is the local voltage drop across the interface and $\Delta\phi_{eq}$ is the Nernst equilibrium voltage. The boundary conditions we applied in dimensionless form are

$$\bar{F}(o,t) = 0,$$
$$\hat{n}\,.\,\bar{F}(1,t) = -\bar{F}_s,$$
$$\hat{n}\,.\,\bar{\nabla}\bar{c}(0,t) = 0,$$
$$\hat{n}\,.\,\bar{\nabla}\bar{c}(1,t) = 0.$$

Transient temperature responses were incorporated into the ROM by an enthalpy balance on the bulk battery. An A123 Systems 26650, 2.3 Ah cylindrical battery was chosen for the study because it is widely studied and property data is readily available. A cylindrical Li-ion battery is fabricated by rolling a stack of cathode/separator/anode layers. The individual layered sheets are thin, and lumped parameters are used so material properties such as the thermal conductivity, density, and specific heat capacity are assumed to be constant in a homogeneous and isotropic body. The thermal conductivity is one or two orders of magnitude higher in the axial direction than in the radial direction resulting in a relatively uniform temperature distribution in the axial direction [42,43]. Also given natural convection the heat transfer at the surface is much smaller than the internal heat transfer by conduction resulting in insignificant temperature gradients inside the battery. Under these assumptions, the energy balance equation in the battery can be described by one bulk volume averaged temperature [44]. To predict the thermal response of the battery we used a simplified energy balance equation for the enthalpy change for electrochemical reactions [45]. Assuming constant system volume and pressure, and neglecting heat generation due to enthalpy-of-mixing, the energy balance equation is expressed as

$$M\,c_p\,\frac{\partial T}{\partial t} = I\left(V_{oc} - T\frac{\partial V_{oc}}{\partial T}\right) - IV + \dot{q}_{\mathrm{sur}} \qquad \text{Eq. 5}$$

where V_{oc} represents the open-circuit voltage (OCV). The OCV is generally a function of the battery state-of-charge (SOC) and temperature (T). The term $IT\frac{\partial V_{oc}}{\partial T}$ is the reversible heat generation and can be calculated from the entropy of reaction [46]. In this study, this reversible heat generation is neglected for simplicity. This simplification is warranted since it is insignificant for the $LIFePO_4$ chemistry [47, 48]. Given this simplification the OCV becomes a function of SOC only and Equation 5 was solved exactly for the battery's temperature response

$$\overline{T}(t) = T_\infty - \frac{e^{-\frac{A_b h_c t}{cp\,\nu\,\rho}}\left(-1+e^{\frac{A_b h_c t}{cp\,\nu\,\rho}}\right)I_b(\overline{V}(T)-\overline{V}oc)}{A_b h_c} \quad \text{Eq. 6}$$

Posing the battery's thermal model in the above manner delegates it's highly nonlinear bulk phase behavior to the enthalpy balance where the particular battery's OCV is utilized. Under the assumption that the ion activity in the electrolyte adjacent to the particle (based on dimensionless ion concentration) is 1.0, $\Delta\phi eq = -\mu/e$ [31]. This gives the voltage profile for the single particle battery $V = V^\theta + \eta - \mu/e$ where V^θ is the standard potential defined by the open circuit voltage plateau (3.42 V vs. Li metal). In terms of the hyperbolic sin and solving for η this gives the voltage of the single particle battery as

$$\overline{V}_{CH}(T) + V^\theta = \overline{\eta} - \frac{\overline{\mu}}{e} = \frac{k_b T}{e}\left(-\overline{\mu} - 2sinh^{-1}\left(\frac{\bar{I}}{\overline{I_0(\bar{c})}}\right)\right). \quad \text{Eq. 7}$$

While it is widely believed that phase separation is suppressed in the typical operation of $LiFePO_4$ batteries, the emergent plateauing effect for the battery voltage response is related to the tendency of $LiFePO_4$ towards phase transition [47]. There appears to be a marked increase towards a typical diffusion-controlled response for the A123 Systems 26650 battery for lower ambient temperatures reminiscent of the COMSOL simulations in Figure 3.

Simulation Results / Discussion

The Cahn-Hilliard SP model is a fourth-order partial differential equation in concentration, so casting it directly in the weak form results in second order spatial derivatives in the weak formulation. Our model resolves this by rephrasing the problem in COMSOL Multiphysics' standard PDF format as a system of two coupled second order PDEs in ion concentration and chemical potential respectively [32].

Parameter studies were conducted for conditions producing enthalpies of mixing resulting in repulsive and attractive forces between Li+ ions and vacancies. When the particle repulses the added ion ($\bar{\Omega} < 0$) or when the ion is attracted but $T > T_c = \bar{\Omega}/2\ k_b$ phase separation is not expected to occur. For these cases, the intercalation process is a simple nonlinear diffusion of the ion. Battery voltage profiles for repulsive behavior ($\bar{\Omega} = -2$) shown in Figure2 were similar to simple diffusion or shrinking core model responses

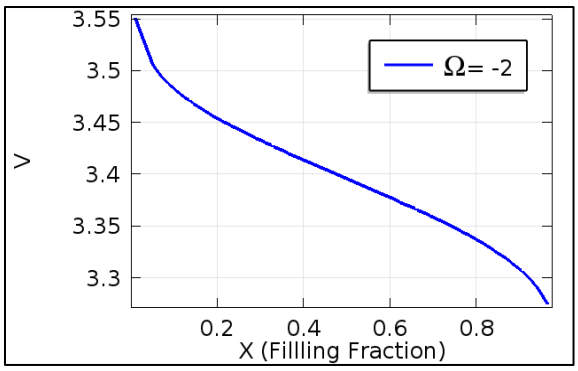

Figure 2: Voltage vs. filling fraction with mixing enthalpy = -2.

Enthalpies in the attractive range, result in much different results from the simple diffusion behavior in Figure 2. Figure 3 shows discharge curves for the attractive cases $\bar{\Omega}$ = 1 and 2. For these values even though there is no phase change there is significant plateauing of the discharge response.

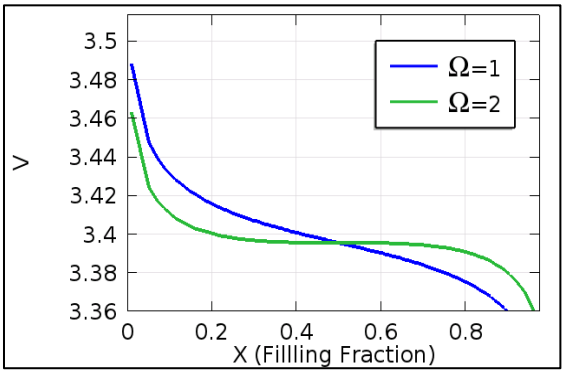

Figure 3: Voltage vs. filling fraction with mixing enthalpies 1 and 2.

and increasing $\bar{\Omega}$ results in a rotation of the voltage response about the half-filled particle concentration. For mixing enthalpies > 2, phase separation can theoretically occur. This behavior is shown in Figures 4 and 5 for $\bar{\Omega}$ = 2.5. Spinodal phase decomposition results in a sudden increase in voltage at the onset of two-phase behavior. Thereafter the voltage is effectively constant until the solution once again becomes a single high concentration phase.

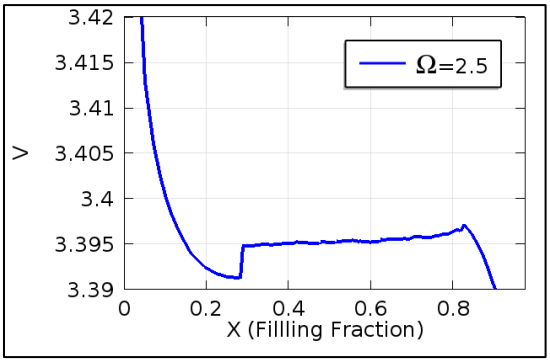

Figure 4: Voltage vs. filling fraction for solid solution with $\Omega = 2.5$.

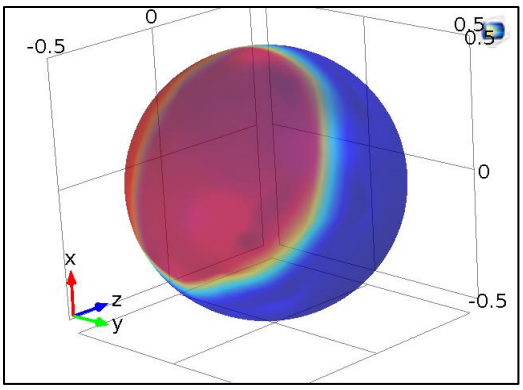

Figure 5: Dimensionless ion surface concentration for $\Omega = 2.5$.

Data sets for the RHS of Equation 7 for thermal embedding were generated by fitting T_∞ = 253, 273 and 298 K corresponding to the A123 Systems 26650 battery data sheet. Temperature profiles from the bulk battery enthalpy balance were incorporated into the energy term in Equation 7 and the exchange current density term in Equation 7 was fitted to the datasheet voltages at 50 percent SOC corresponding to the half-filled single particle according to fraction of filling (x_f) defined as

$$x_f = \frac{\int c\, dV}{\frac{4}{3}\pi R_P^3\, c_m}. \quad \text{Eq. 8}$$

The dataset consisted of one hundred values of the RHS of Equation 7 as a function of SOC and T_∞ and

$$A = \begin{bmatrix} -V^\theta + \frac{k_b T}{e}\left(-\bar{\mu} - 2\sinh^{-1}\left(\frac{\bar{I}}{2\bar{I}_0}\right)_{298_1}\right) & \dots & -V^\theta + \frac{k_b T}{e}\left(-\bar{\mu} - 2\sinh^{-1}\left(\frac{\bar{I}}{2\bar{I}_0}\right)_{253_1}\right) \\ -V^\theta + \frac{k_b T}{e}\left(-\bar{\mu} - 2\sinh^{-1}\left(\frac{\bar{I}}{2\bar{I}_0}\right)_{298_2}\right) & \dots & -V^\theta + \frac{k_b T}{e}\left(-\bar{\mu} - 2\sinh^{-1}\left(\frac{\bar{I}}{2\bar{I}_0}\right)_{253_2}\right) \\ \vdots & \vdots & \vdots \\ -V^\theta + \frac{k_b T}{e}\left(-\bar{\mu} - 2\sinh^{-1}\left(\frac{\bar{I}}{2\bar{I}_0}\right)_{298_{99}}\right) & \dots & -V^\theta + \frac{k_b T}{e}\left(-\bar{\mu} - 2\sinh^{-1}\left(\frac{\bar{I}}{2\bar{I}_0}\right)_{253_{99}}\right) \\ -V^\theta + \frac{k_b T}{e}\left(-\bar{\mu} - 2\sinh^{-1}\left(\frac{\bar{I}}{2\bar{I}_0}\right)_{298_{100}}\right) & \dots & -V^\theta + \frac{k_b T}{e}\left(-\bar{\mu} - 2\sinh^{-1}\left(\frac{\bar{I}}{2\bar{I}_0}\right)_{253_{100}}\right) \end{bmatrix}$$

test battery datasheet voltage profiles were sampled for the same SOC and x_f values.

$$V = \begin{bmatrix} V_{298_1} & V_{273_1} & V_{253_1} \\ V_{298_2} & V_{273_2} & V_{253_2} \\ \vdots & \vdots & \vdots \\ V_{298_{99}} & V_{273_{99}} & V_{253_{99}} \\ V_{298_{100}} & V_{273_{100}} & V_{273_{100}} \end{bmatrix}.$$

A was decomposed by Singular Value Decomposition as $A = U{\cdot}\Sigma{\cdot}V^T$. Figures 6 and 7 show the results for retaining two and one singular values respectively. There was an insignificant improvement of the model fit for over two singular values but retaining only one is inadequate for fitting the experimental battery discharge data. The magnitude of the singular value associated with 253 K >> 273 K>>298 K.

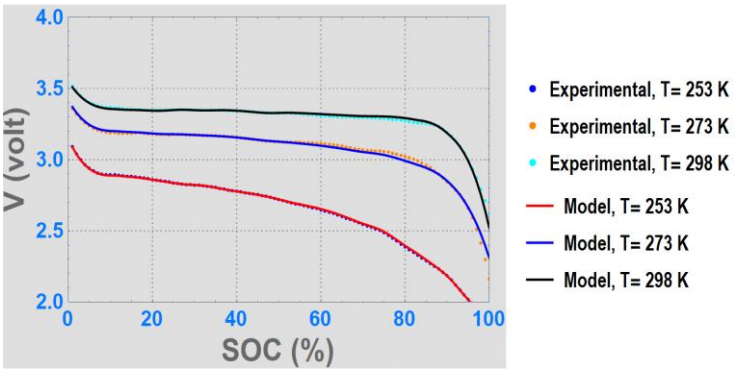

Figure 6: Voltage SOC Response with two Singular Values.

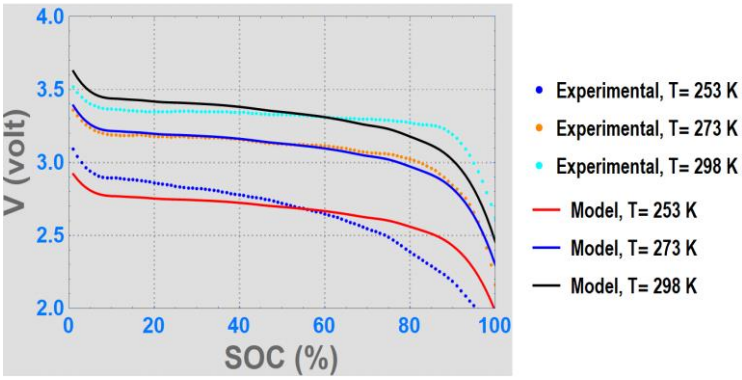

Figure 7: Voltage SOC Response with 0ne Singular Value.

According to Eckart-Young theorem the resulting A_k with numerical rank k = 2 is the best low rate matrix for fitting the battery spread sheet data. To generalize the model for any temperature over the batteries operating range the pseudoinverse was used to solve for the vector X.

$$\mathbf{X = V.PseudoInverse[A_k]}$$

The vector X was then decomposed to include the product of a diagonal matrix and a 2D rotation matrix.

$$V(T) = X'{\cdot}A_\perp{\cdot}\begin{bmatrix} S_T & 0 & 0 \\ 0 & S_{253} & 0 \\ 0 & 0 & S_{273} \end{bmatrix}\cdot\begin{bmatrix} Cos(\theta_T) & -Sin(\theta_T) \\ Sin(\theta_T) & Cos(\theta_T) \end{bmatrix}$$

Where $\boldsymbol{S_T}$ and $\boldsymbol{\theta_T}$ are simple second order interpolations of temperature (T) specific to the A123 Systems 26650 battery.

$$\boldsymbol{S_T = 0.0000053467\,T^2 - 0.00308735\,T + 0.44286}$$
$$\boldsymbol{\theta_T = -0.000019333\,T^2 + 0.13319\,T - 1.19228}$$

The final fit of the model is shown in Figure 8 for the spread sheet temperatures and intermediate temperatures 263 and 285 K.

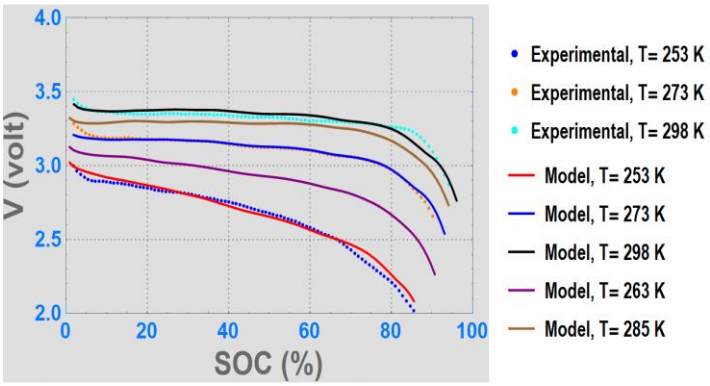

Figure 8: Voltage SOC Response for the ROM Thermal Model

Conclusion

There is no existing theory for simply "scaling-up" Cahn Hilliard single particle models to reflect bulk battery behavior. We do not make inferences as to the actual magnitudes of the meso-scale parameters. However, our statistical approach based on singular value decomposition and principal component regression incorporates Cahn-Hilliard single particle simulation results by fitting low order temperature dependent parameters in hyperspace. We present our model as the lowest order thermal model cable of statistically modelling the emergent voltage plateauing of $LiFePO_4$ batteries and more significantly the transition between plateauing and diffusion like voltage responses. The resulting ROM is computationally competitive with existing ECMs and is unique in its ability to simulate emergent SP properties in a full-scale battery thermal model.

References

1. Larcher, D.; Tarascon, J. Towards Greener and More Sustainable Batteries for Electrical Energy Storage. *Nature Chemistry* 2014, *7*, 19-29.
2. Manzetti, S.; Mariasiu, F. Electric Vehicle Battery Technologies: From Present State to Future Systems. *Renewable and Sustainable Energy Reviews* 2015, *51*, 1004-1012.
3. Scrosati, B.; Garche, J. Lithium Batteries: Status, Prospects and Future. *Journal of Power Sources* 2010, *195*, 2419-2430.
4. Fergus, J. Recent Developments in Cathode Materials for Lithium Ion Batteries. *Journal of Power Sources* 2010, *195*, 939-954.
5. Parrett, T. (2016, March 09). Batteries That Will Save the Planet. Retrieved from https://www.newsweek.com/2014/12/26/batteries-will-save-planet-291528.html
6. Shim, J. (2002). Electrochemical analysis for cycle performance and capacity fading of a lithium-ion battery cycled at elevated temperature. *Journal of Power Sources,112*(1), 222-230. doi:10.1016/s0378-7753(02)00363-4
7. Tobishima, S., & Yamaki, J. (1999). A consideration of lithium cell safety. *Journal of Power Sources,81-82*, 882-886. doi:10.1016/s0378-7753(98)00240-7
8. Spotnitz, R., & Franklin, J. (2003). Abuse behavior of high-power, lithium-ion cells. *Journal of Power Sources,113*(1), 81-100. doi:10.1016/s0378-7753(02)00488-3
9. Yannliaw, B. (2004). Modeling of lithium ion cells?A simple equivalent-circuit model approach. *Solid State Ionics,175*(1-4), 835-839. doi:10.1016/j.ssi.2004.09.049
10. Verbrugge, M. (2007). Adaptive, multi-parameter battery state estimator with optimized time-weighting factors. *Journal of Applied Electrochemistry,37*(5), 605-616. doi:10.1007/s10800-007-9291-7
11. Hu, Y., Yurkovich, S., Guezennec, Y., & Yurkovich, B. (2011). Electro-thermal battery model identification for automotive applications. *Journal of Power Sources,196*(1), 449-457. doi:10.1016/j.jpowsour.2010.06.037
12. Perez, H. E., Siegel, J. B., Lin, X., Stefanopoulou, A. G., Ding, Y., & Castanier, M. P. (2012). Parameterization and Validation of an Integrated Electro-Thermal Cylindrical LFP Battery Model. *Volume 3: Renewable Energy Systems; Robotics; Robust Control; Single Track Vehicle Dynamics and Control; Stochastic Models, Control and Algorithms in Robotics; Structure Dyna-mics and Smart Structures;*. doi:10.1115/dscc2012-movic2012-8782
13. Torabi F, Ahmadi P. *Simulation Of Battery Systems*. London: Academic Press; 2019.
14. Barreras, Jorge Varela, et al. "Datasheet-Based Modeling of Li-Ion Batteries." *2012 IEEE Vehicle Power and Propulsion Conference*, 2012, doi:10.1109/vppc.2012.6422730.
15. Santhanagopalan, S.; Guo, Q.; Ramadass, P.; White, R. Review of Models for Predicting the Cycling Performance of Lithium Ion Batteries. *Journal of Power Sources* 2006, *156*, 620-628.
16. Ning, G.; Popov, B. Cycle Life Modeling of Lithium-Ion Batteries. *Journal of The Electrochemical Society* 2004, *151*, A1584.
17. Guo, M.; Sikha, G.; White, R. Publisher'S Note: Single-Particle Model for A Lithium-Ion Cell: Thermal Behavior [J. Electrochem. Soc., 158, A122 (2011)]. *Journal of The Electrochemical Society* 2011, *158*, S11.
18. Cai, L.; White, R. Mathematical Modeling of a Lithium Ion Battery with Thermal Effects in COMSOL Inc. Multiphysics (MP) Software. *Journal of Power Sources* 2011, *196*, 5985-5989.
19. Painter, R., Berryhill, B., Sharpe, L., and Hargrove, S. K., *A Single Particle Thermal Model for Lithium Ion Batteries*, Proceedings of the 2012 COMSOL Conference Boston, MA.
20. Padhi, A. K. (1997). Phospho-olivines as Positive-Electrode Materials for Rechargeable Lithium Batteries. *Journal of The Electrochemical Society,144*(4), 1188. doi:10.1149/1.1837571
21. Yamada, A., Chung, S. C., & Hinokuma, K. (2010). ChemInform Abstract: Optimized $LiFePO_4$ for Lithium Battery Cathodes. *ChemInform,32*(29). doi:10.1002/chin.200129017
22. Huang, H., Yin, S., & Nazar, L. F. (2001). Approaching Theoretical Capacity of $LiFePO_4$ at Room Temperature at High Rates. *Electrochemical and Solid-State Letters,4*(10). doi:10.1149/1.1396695

23. Ravet, N., Chouinard, Y., Magnan, J., Besner, S., Gauthier, M., & Armand, M. (2001). Electroactivity of natural and synthetic triphylite. *Journal of Power Sources,97-98*, 503-507. doi:10.1016/s0378-7753(01)00727-3
24. Chung, S., Bloking, J. T., & Chiang, Y. (2002). Electronically conductive phospho-olivines as lithium storage electrodes. *Nature Materials,1*(2), 123-128. doi:10.1038/nmat732
25. Johns, P. A., Roberts, M. R., Wakizaka, Y., Sanders, J. H., & Owen, J. R. (2009). How the electrolyte limits fast discharge in nanostructured batteries and supercapacitors. *Electrochemistry Communications,11*(11), 2089-2092. doi:10.1016/j.elecom.2009.09.001
26. Srinivasan, V.; Newman, J. Discharge Model for The Lithium Iron-Phosphate Electrode. *Journal of The Electrochemical Society* 2004, *151*, A1517.
27. Newman, J.; Tiedemann, W. Porous-Electrode Theory with Battery Applications. *AIChE Journal* 1975, *21*, 25-41.
28. Doyle, M. Modeling of Galvanostatic Charge and Discharge of the Lithium/Polymer/Insertion Cell. *Journal of The Electrochemical Society* 1993, *140*, 1526.
29. Bazant, M. Theory of Chemical Kinetics and Charge Transfer Based on Nonequilibrium Thermodynamics. *Accounts of Chemical Research* 2013, *46*, 1144-1160.
30. Singh, G., Ceder and Bazant, M., *Intercalation dynamics in rechargeable battery materials: General theory and phase-transformation waves in LiFePO$_4$*, Electrochimica Acta 53, 7599-7613 (2008).
31. Zeng, Y.; Bazant, M. Cahn-Hilliard Reaction Model for Isotropic Li-Ion Battery Particles. *MRS Proceedings* 2013, *1542*.
32. Bai, P.; Cogswell, D.; Bazant, M. Z. Suppression of ~~phase separation~~ faze separation in LiFePO$_4$ nanoparticles during battery discharge
33. Painter, R.; Sharpe, L.; Hargrove, S.K., *A Phase Field Model for Lithium Batteries*, Proceedings of the 2012 COMSOL Conference Boston, MA.
34. Malik R, Abdellahi A, Ceder G. A Critical Review of the Li Insertion Mechanisms in LiFePO$_4$Electrodes. *J Electrochem Soc*. 2013;160(5):A3179-A3197. doi:10.1149/2.029305jes
35. Sullivanuv.com. http://www.sullivanuv.com/wp-content/uploads/2014/06/A123-Cell-Datasheet-2008-08.pdf. Published 2019. Accessed December 1, 2019.
36. Keizer J. *Statistical Thermodynamics Of Nonequilibrium Processes*. New York: Springer-Verlag; 1987.
37. Laughlin R, Pines D, Schmalian J, Stojkovic B, Wolynes P. The middle way. In: *Proceedings Of The National Academy Of Sciences*. ; 2000:97 (1) 32-37; DOI: 10.1073/pnas.97.1.32.
38. *Mahler G. Quantum Thermodynamic Processes: Energy and Information Flow at the Nanoscale*. Singapore: Pan Stanford Publishing; 2015.
39. Maleki H. Thermal Properties of Lithium-Ion Battery and Components. *J Electrochem Soc*. 1999;146(3):947. doi:10.1149/1.1391704
40. Chen Y. Thermal Analysis of Lithium-Ion Batteries. *J Electrochem Soc*. 1996;143(9):2708. doi:10.1149/1.1837095
41. Onda K, Ohshima T, Nakayama M, Fukuda K, Araki T. Thermal behavior of small lithium-ion battery during rapid charge and discharge cycles. *J Power Sources*. 2006;158(1):535-542. doi:10.1016/j.jpowsour.2005.08.049
42. Bernardi D. A General Energy Balance for Battery Systems. *J Electrochem Soc*. 1985;132(1):5. doi:10.1149/1.2113792
43. Thomas K, Newman J. Thermal Modeling of Porous Insertion Electrodes. *J Electrochem Soc*. 2003;150(2):A176. doi:10.1149/1.1531194
44. Forgez C, Vinh Do D, Friedrich G, Morcrette M, Delacourt C. Thermal modeling of a cylindrical LiFePO$_4$/graphite lithium-ion battery. *J Power Sources*. 2010;195(9):2961-2968. doi:10.1016/j.jpowsour.2009.10.105
45. Youngki K. *Power Capability Estimation Accounting for Thermal and Electrical Constraints for Lithium-Ion Batteries.* University of Michigan, Ph.D. Dissertation; 2014.
46. Ferguson T. *Lithium-ion Battery Modeling Using Non-Equilibrium Thermodynamics.* Massachusetts Institute of Technology, Ph.D., Dissertation; 2014.
47. Orvananos B, Ferguson T, Yu H, Bazant M, Thornton K. Particle-Level Modeling of the Charge-Discharge Behavior of Nanoparticulate Phase-Separating Li-Ion Battery Electrodes. *J Electrochem Soc*. 2014;161(4):A535-A546. doi:10.1149/2.024404jes